

JGR Space Physics

RESEARCH ARTICLE

10.1029/2022JA030438

†Retired, Pasadena, CA, USA

Key Points:

- Type 1 upper band chorus and gap chorus are found to be composed of short duration subelements which are monochromatic ($\sigma \leq 1\%$)
- Since all parts of chorus risers have similar constructions, it is most probable that they are generated by anisotropic narrow energy-range phase-bunched electrons
- A Type 2 chorus (no connection between the lower band and upper band) was studied. The upper band was composed of monochromatic subelements

Supporting Information:

Supporting Information may be found in the online version of this article.

Correspondence to:

B. T. Tsurutani,
bruce.tsurutani@gmail.com

Citation:

Chen, R., Tsurutani, B. T., Gao, X., Lu, Q., Chen, H., Lakhina, G. S., & Hajra, R. (2022). The structure and microstructure of rising-tone chorus with frequencies crossing at $f \sim 0.5 f_{ce}$. *Journal of Geophysical Research: Space Physics*, 127, e2022JA030438. <https://doi.org/10.1029/2022JA030438>

Received 4 MAR 2022

Accepted 15 JUL 2022

The Structure and Microstructure of Rising-Tone Chorus With Frequencies Crossing at $f \sim 0.5 f_{ce}$

Rui Chen^{1,2,3} , Bruce T. Tsurutani[†] , Xinliang Gao^{1,2,3} , Quanming Lu^{1,2,3} , Huayue Chen^{1,2,3} , Gurbax S. Lakhina⁴, and Rajkumar Hajra⁵ 

¹CAS Key Laboratory of Geospace Environment, School of Earth and Space Sciences, University of Science and Technology of China, Hefei, China, ²CAS Center for Excellence in Comparative Planetology, Hefei, China, ³Collaborative Innovation Center of Astronautical Science and Technology, Harbin, China, ⁴Indian Institute of Geomagnetism, Navi Mumbai, India, ⁵Indian Institute of Technology Indore, Indore, India

Abstract Intense, midnight-to-dawn sector, near-equatorial, chorus rising tones which cross frequencies of $\sim 0.5 f_{ce}$ have been analyzed to determine their structures and possible substructures. Upper band ($f \geq 0.5 f_{ce}$) chorus and “gap” ($f \sim 0.5 f_{ce}$) chorus are examined in detail for the first time. It is found that upper band chorus and gap chorus are composed of the same structure as lower band ($f \leq 0.5 f_{ce}$) chorus: they are composed of short-duration subelements, which are monochromatic with $\sigma \leq 1\%$. These findings have strong implications for the chorus element generation mechanism. Following Kennel and Petschek (1966, <https://doi.org/10.1029/JZ071i001p00001>) the overall chorus riser is most likely generated by anisotropic ($T_\perp/T_\parallel > 1$) $\sim 10\text{--}100$ keV substorm-injected electrons. Assuming cyclotron resonance, the upper band chorus is generated by the low energy portion of the electron spectrum. The often-present gap at $\sim 0.5 f_{ce}$ is related to Landau/cyclotron damping. This however is not the end of the story. There is another type of two-frequency chorus (called Type 2) for which the lower band is not well connected to the upper band. A Type 2 chorus reported previously by Fu et al. (2014, <https://doi.org/10.1002/2014JA020364>) has also been studied in detail. Both the lower band and upper band are composed of subelements which are monochromatic. Such a similar fine structure for the different type of chorus may imply a similar generation mechanism, for which the difference between them is just the energy range of resonant energetic electrons. One mechanism discussed here, generation by phase bunched electrons, will be tested in the near future.

Plain Language Summary Understanding chorus structure and microstructure is essential toward understanding the wave generation mechanisms and wave-particle interaction consequences. In this paper we show that upper band ($f \geq 0.5 f_{ce}$) chorus and gap chorus ($f \sim 0.5 f_{ce}$) are composed of substructures (subelements) which are monochromatic with $\sigma \leq 1\%$. These are the same features of lower band ($f \leq 0.5 f_{ce}$) chorus. The Kennel-Petschek theory therefore needs to be enlarged such that phase-bunching of $\sim 10\text{--}100$ keV substorm injected anisotropic electrons occur, which then “lase” to yield the monochromatic wave subelements. Coherent and monochromatic chorus can explain the rapid burstiness of ionospheric microburst X-ray structures. There is another type of upper band chorus, called Type 2 upper band chorus, where the lower band chorus elements are not clearly connected to the upper band chorus. A Type 2 chorus reported previously by Fu et al. (2014, <https://doi.org/10.1002/2014JA020364>) has been examined in this paper. The apparently unrelated upper band has been found to be composed of subelements which are monochromatic in nature. Thus the different type of chorus may be excited by a similar generation mechanism, for which the difference between them is only the energy interval of the resonant energetic electrons.

1. Introduction

Electromagnetic whistler-mode chorus was first observed in space by Russell et al. (1969) using Orbiting Geophysical Observatory-3 (OGO-3) triaxial search coil spectrum channel data. Burtis and Helliwell (1969) using single aircore loop antennas placed on both OGO-1 and -3 discovered that chorus in space often had two frequency bands. Tsurutani and Smith (1974) supplementing the OGO-5 triaxial search coil wideband data with dc magnetometer data showed that the two-frequency chorus bands were separated by a gap at $\sim 0.5 f_{ce}$, where f_{ce} is the electron cyclotron frequency. In this paper, we will hereafter refer to these two parts of chorus as “lower band chorus” ($f < 0.5 f_{ce}$) and “upper band chorus” ($f > 0.5 f_{ce}$), respectively. Occasionally chorus is detected at $f \sim 0.5 f_{ce}$. This will be called “gap” chorus.

Several mechanisms explaining the generation of upper band chorus and the power gap at $f \sim 0.5f_{ce}$ have been developed in the past decades (Bell et al., 2009; Chen et al., 2021; Coroniti et al., 1984; Fu et al., 2014; Gao et al., 2016, 2019; Kurita et al., 2012; Li et al., 2019; Liu et al., 2011; Maeda, 1976; Omura, 2021; Omura et al., 2009; Ratcliffe & Watt, 2017; Schriver et al., 2010; Teng et al., 2019; Tsurutani & Smith, 1974). Tsurutani and Smith (1974), Coroniti et al. (1984) and Omura et al. (2009) have argued that the rising tone emissions are all connected (across the $0.5f_{ce}$ gap) to upper band chorus elements with the waves around $0.5f_{ce}$ experiencing severe damping. Santolík et al. (2003) and Li et al. (2011) have indicated that upper band chorus propagates at slightly oblique angles to the ambient magnetic field. This is in agreement with the Omura et al. (2009) nonlinear Landau damping mechanism away from the equator. In a slight variation of the above scenarios, Fu et al. (2014) believe that two distinct anisotropic electron components with significantly different temperatures are generating the two bands of chorus. For this case, there should not be a relationship between the lower band chorus and the upper band chorus. Chen et al. (2021, 2022a) have suggested that the Landau accelerated low energy electron beam causes further cyclotron damping of the $\sim 0.5f_{ce}$ waves at the equator, so both Landau and cyclotron damping are involved.

On the other hand, others have argued that the upper band chorus is generated by a different mechanism than lower band chorus. Maeda (1976) believe that the lower band chorus is not connected to upper band chorus and instead the upper band emissions are electrostatic modes generated by $\sim 1\text{--}5$ keV magnetic storm injected electrons. Gao et al. (2016, 2019) reported a type of two frequency chorus where the lower band was electromagnetic and the upper band was electrostatic, in partial agreement with Maeda (1976). Gao et al. (2016) believe that the upper band is generated by wave-wave coupling between lower band chorus and a density mode creating an upper band of chorus at twice the frequency of the lower band. They also noted that the gap was not always at $\sim 0.5f_{ce}$. Liu et al. (2011) have argued that “both the lower and the upper bands can be generated simultaneously by the whistler anisotropy instability driven by two bi-Maxwellian electron components.” “The upper band can be excited by anisotropic electrons below ~ 1 keV.” Teng et al. (2019) dispute the Liu et al. mechanism because they note for this to work there should be a gap in the anisotropy of intermediate energy (~ 1 keV) hot electron population. Teng et al. observed magnetic local time (MLT) distributions of banded and no-gap chorus are opposite to what is expected from the Liu et al. (2011) model. Li et al. (2019) have a different model still. They believe that the anisotropic electrons generate a broad frequency range of chorus and through Landau resonance electrons are accelerated. The electrons create new chorus waves in both the upper band and lower band ranges. Tsurutani and Smith (1974) in their Figure 3 showed an extended chorus example where the upper band chorus was only loosely related to lower band chorus and the simple explanation of cyclotron or Landau damping cannot be used (to emphasize this point the figure is reproduced in Figure 2). For this case there must be a separate generation mechanism for the upper band chorus.

Tsurutani et al. (1979), Meredith et al. (2001) and Kurita et al. (2012) showed that the free energy associated with chorus generation was substorm injection of anisotropic ($T_{\perp}/T_{\parallel} > 1$) energetic substorm electrons. T_{\perp} and T_{\parallel} are the perpendicular and parallel electron temperatures with respect to the ambient magnetic field, following the Quasi-Linear theory of Kennel and Petschek (1966). See also Liu et al. (2011) and Fu et al. (2014). In the intervening years, focus has been primarily put on the lower band emissions since they resonate with the highest energy electrons and cause the diffuse aurora (Thorne et al., 2010).

Santolík et al. (2003) showed that low frequency chorus riser elements were composed of “packets” or subelements. Tsurutani et al. (2009) showed that the chorus subelements were coherent and significant modifications of Quasi-Linear theory were needed to explain microburst precipitation (Bellan, 2013; Hosokawa et al., 2020; Lakhina et al., 2010; Tsurutani et al., 2013).

Part of the problem for understanding the source of upper band chorus is that many researchers have not understood that there are at least two possible types of upper band chorus. Figures 1 and 2 presents two chorus events with both upper and lower bands. The inset in Figure 1 shows rising tone elements with a gap and then dot-like emissions at higher frequencies. The dot-like emissions seem to be connected to the lower frequency rising tone emissions but with a gap near $0.5f_{ce}$. This data was taken on 15 August 1968 at a $L = 5.9$ and magnetic latitude (MLAT) = -4.2° . The local time was 1.3 hr. We will call these events “Type 1 upper band chorus” in this paper.

The data in Figure 2 was taken on 10 August 1968 at a MLAT = -0.2° , $L = 7.6$ and a local time of 1.1 hr. This is an example of lower-band structureless chorus (hiss-like emissions) separated by $\sim 10\text{--}30$ s (quasi-periods).

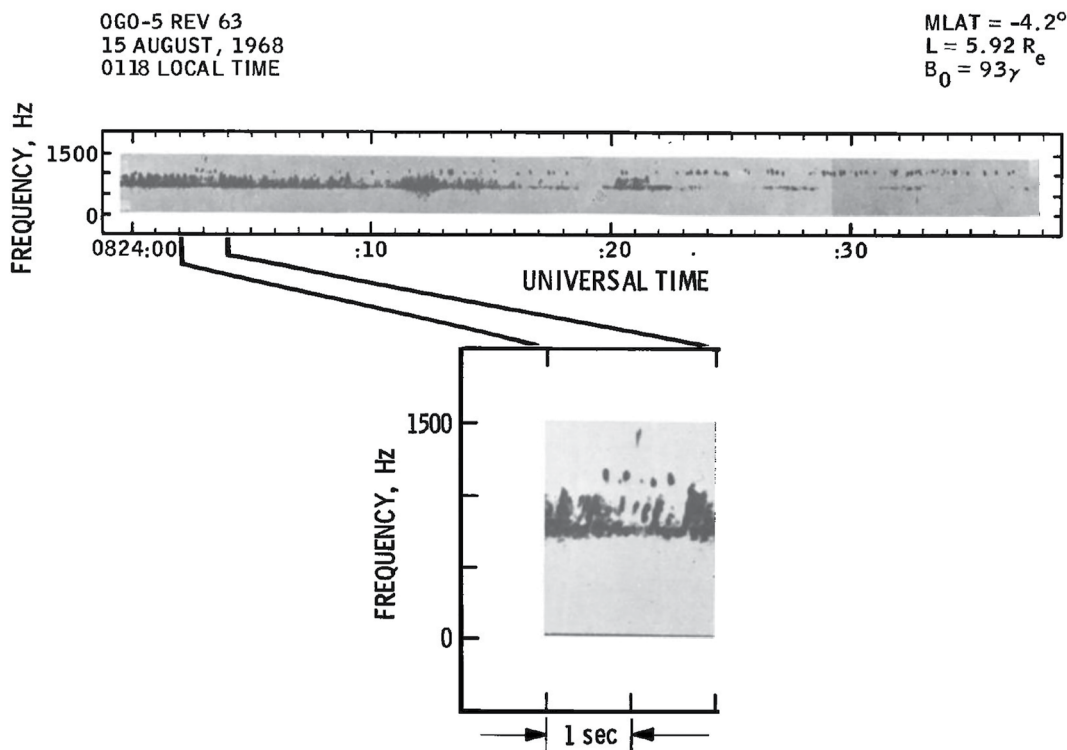


Figure 1. An example of “Type 1” two frequency chorus. From the inset, the lower band emission rises from ~ 700 to $\sim 1,000$ Hz and the upper band is at $\sim 1,150$ Hz, consisting of ~ 0.1 s duration dot-like emissions. There is a strong extinction in the frequency range from $\sim 1,000$ to $1,100$ Hz. The extinction occurs at $f = \sim 0.5f_{ce}$. The lower frequency rising tones in the inset appear to connected to the upper band dots but with a gap at $\sim 0.5f_{ce}$. Taken from Tsurutani and Smith (1974, Figure 6).

Each of the hiss-like emissions were followed by upper-band falling tone emissions. In the inset, the falling tones were delayed by several seconds. The two bands were separated by $f \sim 0.5f_{ce}$. The structure of the upper band chorus is obviously different than that of the lower band chorus/hiss. We will call these types of events “Type 2 upper band chorus.”

It is a strong possibility that the Type 2 events are caused by a different mechanism than Type 1 events. We have performed an extensive search for both Type 1 and Type 2 upper band chorus in the Van Allen Probes plasma wave data. Type 1 upper band chorus is quite common and is the typical case of two-frequency chorus. However a similar case of Type 2 chorus as in Figure 2 was not found in the Van Allen Probes plasma wave data. We therefore will reanalyze the Fu et al. (2014) Type 2 chorus.

2. Data Source and Analysis Method

The OGO-5 satellite was placed in a highly eccentric orbit with a period of ~ 62 hr, a geocentric apogee of $24 R_E$ and an inclination of $\sim 30^\circ$ relative to the geographic equator. The instrument was a triaxial search coil magnetometer where the sensors were located on a boom ~ 7 m from the spacecraft body. The data were taken in analog format. The broadband analog voltages with frequencies from 1 to 1,500 Hz modulated standard Inter Range Instrumentation Group (IRIG) wide band subcarrier oscillators which were then multiplexed and transmitted by special purpose telemetry. A more complete instrument description can be found in Frandsen et al. (1969).

Van Allen Probes (also known as the Radiation Belt Storm Probes/RBSP) were operating in a near-equatorial, highly elliptical, and low-inclination orbit with a perigee of $\sim 1.1 R_E$ and apogee of $\sim 5.8 R_E$. The Electric and Magnetic Field Instrument Suite and Integrated Science (EMFISIS) wave instrument (Kletzing et al., 2013) onboard the satellite provides high-resolution, continuous burst waveform data (35,000 samples/sec) which are analyzed to obtain wave polarization information (such as the wave normal angle and Poynting flux) and wave

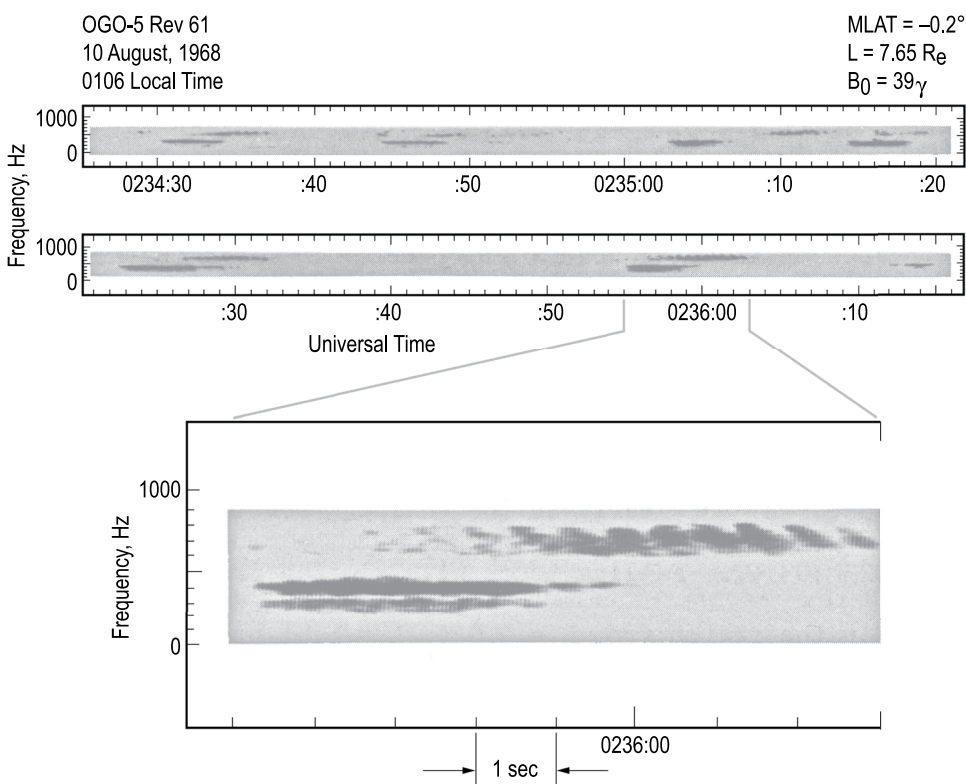


Figure 2. An example of “Type 2” two-frequency chorus. The lower band emissions (~ 300 – 500 Hz) presented as hiss-like nature occur at quasi-periodic intervals of ~ 10 – 30 s. The upper band chorus (~ 675 – 850 Hz) occurs following the lower band chorus with a delay of several seconds. The gap between the two bands from ~ 500 to 675 Hz is at $f \sim 0.5f_{ce}$. This is an example of Type 2 upper band chorus. The figure is taken from Tsurutani and Smith (1974, Figure 3).

structure (subelement property) information. The triaxial fluxgate magnetometer (MAG, a part of the EMFISIS instrument suite) was used to obtain the direction and magnitude of the local background magnetospheric magnetic field. We use the d.c. magnetic field in two different ways in this paper. The d.c. field direction is used to determine the obliqueness of wave propagation relative to the ambient field. The d.c. field magnitude is also used to determine the equatorial electron cyclotron frequency, f_{ce} . This method is described below.

In all of our chorus cases studied, we first note the measured magnetic field magnitude and the location of the spacecraft in MLAT. Based on a dipole magnetic field model, the magnitude of the magnetic field at equator (B_{eq}) can be estimated using the local magnetic field (B_{loc}) and MLAT (λ) of the satellite, that is, $B_{eq} = B_{loc}\cos^6\lambda/\sqrt{1+3\sin^2\lambda}$. We then determine the equatorial electron cyclotron frequency f_{ce} by this simple extrapolation (Gao et al., 2016; Li et al., 2019). This technique combines both measurement and modeling so it will be described as “measuredmodeled” in this paper.

We have selected chorus riser elements located between local midnight and 06 MLT. This is the region where the substorm injected energetic electron cloud will gradient and curvature drift from midnight to dawn in the magnetosphere. We have also restricted the MLAT location of chorus to within $\pm 10^\circ$ of the magnetic equator, the generation region of chorus (Lauben et al., 2002; LeDocq et al., 1998; Meredith et al., 2001; Tsurutani & Smith, 1974, 1977).

For the analyses of the high time resolution electromagnetic field data, we use the Sonnerup and Cahill (1967) minimum variance technique applied to the electromagnetic plasma waves (Smith & Tsurutani, 1976). The magnetic field component of the wave along the maximum variance direction will be called the B1 component, the one along the intermediate variance direction B2, and the one along the minimum variance direction B3. The minimum variance direction of the magnetic component of chorus waves is the direction of wave propagation k (Verkhoglyadova et al., 2010). We have used the Space Physics Environment Data Analysis Software (SPEDAS)

bandpass filter to obtain the waveform signatures in the specific frequency ranges (i.e., $\sim 0.1\text{--}0.5f_{ce}$ for lower band chorus and $\sim 0.5\text{--}0.75f_{ce}$ for upper band chorus). The specific frequency ranges chosen will be indicated in the figure captions to follow.

We use the zero crossings of the B1 component to identify the start and stop times of the half wave cycles. The wave “frequency” for each half cycle is calculated based on the time interval between the start and stop times. It has been shown both observationally (Tsurutani et al., 2009) and theoretically (Verkhoglyadova et al., 2010) that chorus is a circularly polarized electromagnetic wave. It is therefore immaterial if one uses the B1 or B2 component zero crossings or maxima or minima crossings. Any of these choices will give the same results. For this study we have chosen the B1 half wave zero crossing. It was previously shown in Tsurutani et al. (2020) that the technique worked well (for full wave cycle zero crossings).

In our analyses of chorus wave frequencies, we have only analyzed portions for which the wave amplitudes are the largest. Near the ends of the subelements where the wave amplitudes are diminished, uncertainty errors are larger. Tsurutani et al. (2009) have shown that there is omnidirectional noise of ~ 25 pT amplitudes which may throw off detailed analyses results. These regions have not been analyzed in the main body of the paper. Tsurutani et al. (2020) previously analyzed the substructure of lower band chorus using a continuous wavelet transform (a Morlet mother wavelet function). It was found that this did not give any better information than the method used above. So we have not applied this technique in this paper. A Hilbert transformation on several successive subelements has been applied in previous analyses (Santolík et al., 2014). Large frequency shifts are noted to occur at the edges of the subelements or in-between subelements in Figure 3 of Santolík et al. (2014). However this is not the goal of the present paper. We wish to determine if frequency jumps occur where the wave amplitudes in the subelements are large, in the center of subelements. The present method of calculating the frequency based on B1 zero crossings will be shown to be adequate for this purpose. Besides examining each half cycle of a wave for its frequency, we also calculate the variation of frequencies for a sequence of wave cycles. If the standard deviation (σ) is $\leq 1\%$, we have called these events “monochromatic.” The same method of analysis and definitions were used in Tsurutani et al. (2020) in analyzing lower band chorus.

3. Observational Results

Figure 3 shows an upper band chorus rising tone event at $\sim 21:16$ UT, on 31 March 2013. The spacecraft was at a $L = 5.3$, a MLT of ~ 1.5 hr and a MLAT of -1.8° . There are six major rising tone elements shown in the interval. These repetitive emissions of chorus waves are considered to be related to the injection of energetic electrons from the magnetotail (Chen, Lu, et al., 2022; Gao et al., 2022; Lu et al., 2021). All of the chorus risers began close to $f = \sim 0.5f_{ce}$ ($\sim 2,400$ Hz) and rose to $\sim 0.62f_{ce}$ ($\sim 3,000$ Hz). Figure 3c shows that all six of these major risers were propagating away from the magnetic equator. An interval labeled T1 shown in vertical gray shading has been selected for further analyses.

Interspersed between these six major chorus risers are six lesser intensity risers. These risers start at $\sim 2,600$ Hz and rise to $\sim 3,200$ Hz. What is interesting is that some of these events are propagating in the opposite direction as the main chorus risers. This can be seen in Figure 3c. The first element at ~ 31.2 s is propagating northward (red), the second event at ~ 31.5 s starts out propagating southward (black) and then turns to northward at higher frequencies. The third, fourth and fifth minor risers are propagating northward and the sixth riser at 33.3 s is propagating southward. Although these minor chorus risers are interesting, it is out of scope for the present paper. They will be analyzed in a separate publication.

Figure 4 shows the waveform of the T1 riser element. There are 5 major subelements (Figure 4a). We have selected four subelements indicated by red horizontal bars. The average wave propagation (k) angles of four subelements relative to the ambient magnetic field direction B_0 are $\sim 9.8^\circ$, $\sim 6.2^\circ$, $\sim 9.6^\circ$, and $\sim 7.6^\circ$, respectively. The B1–B2 hodogram on the upper right show that the chorus is circularly polarized, as expected from previous chorus studies (Tsurutani et al., 2009) and theory (Verkhoglyadova et al., 2010). Assuming that the upper band chorus portion of the element rises from $\sim 2,350$ to $\sim 3,050$ Hz in ~ 0.2 s, the chirping rate is $\sim 3,500$ Hz/s.

Figures 4b–4e show that the mean frequency values of the four subelements are $\sim 2,726$, $\sim 2,786$, $\sim 2,836$, and $\sim 2,929$ Hz, respectively. All of the subelements had 16 or 17 cycles selected which were analyzed. The σ standard deviation in frequencies for the four subelements are $\sim 0.5\%$, $\sim 0.6\%$, $\sim 0.5\%$ and $\sim 0.3\%$, respectively. Figure 4b

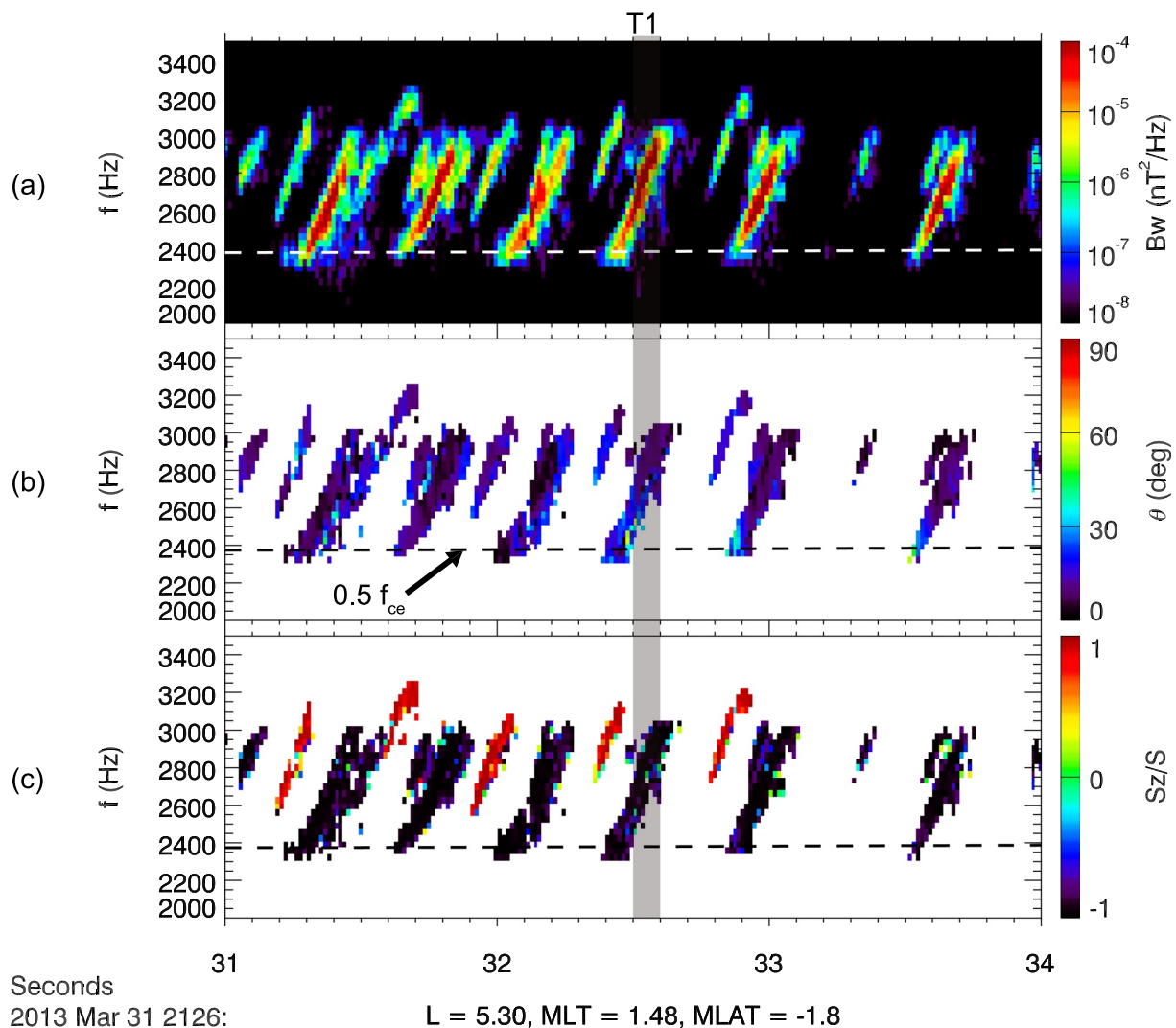


Figure 3. Upper band rising-tone chorus event observed at $\sim 21:26$ UT on 31 March 2013. The panels, from top to bottom are: (a) the wave magnetic power spectrum, (b) the wave normal angle relative to the background magnetic field B_0 , and (c) the ratio S_z/S , where S is the Poynting flux intensity and S_z is its parallel component along B_0 . In each panel, the dashed horizontal line indicates $0.5 f_{ce}$. The color code values are given on the right side of each panel. An interval T1 (vertical gray shading) is selected for detailed analyses later.

shows that the subelement started with slightly higher than average frequencies, dipped to lower than average as the wave intensity peaked, and then ended with slightly higher frequencies. Figure 4c shows that the wave started with the average frequency, then dipped to slightly lower than average frequency in the middle of the subelement and then returned to a slightly higher than average frequency at the end. The subelement in Figure 4d shows slightly below average frequencies at the beginning of the interval and then rising to above average frequencies at the end. The subelement in Figure 4e is similar to the subelement in Figure 4d.

It can be noticed that all of the four subelements Figures 4b–4e have chorus frequencies that vary smoothly from cycle to cycle. All four subelements rose in frequency from the beginning of the interval to the end of the interval, but the rise was not monotonic. Although we have characterized the frequency variation quantitatively by their calculated standard deviation (σ), the wave frequency variations do not appear to be statistical ones, that is, the frequency variation is not a random scattering of a fraction of σ (say $\sim 0.5 \sigma$) from one value to the next. This nature of the frequency variations is not understood at this time. This requires further analysis (and is beyond the scope of the present work).

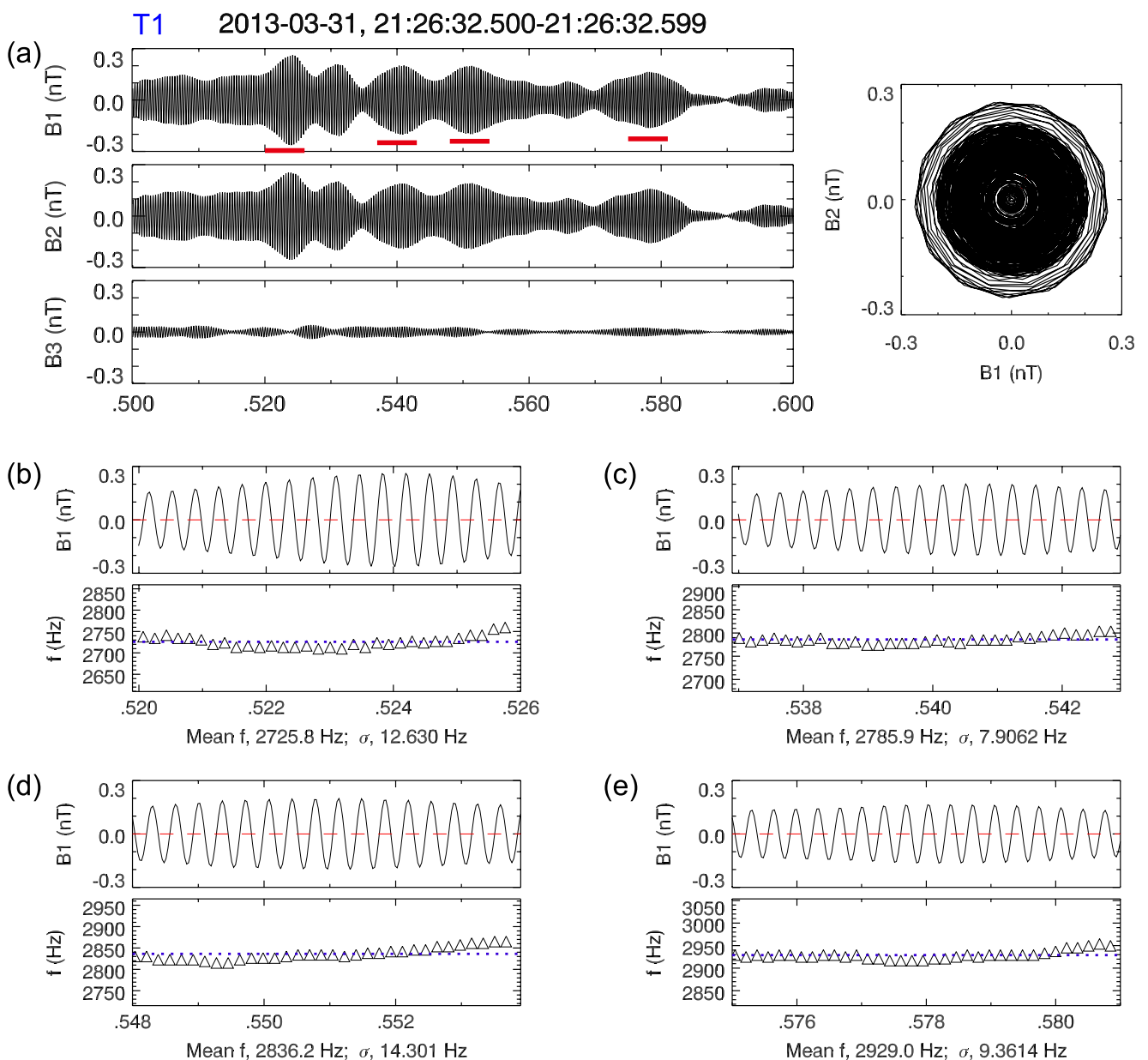


Figure 4. The waveforms of the T1 interval of Figure 3. The frequencies passed through the bandpass filter were selected to be between 2,200 and 3,200 Hz. Panel (a) shows the three minimum variance coordinates B1, B2, and B3. The hodogram between B2 and B1 is shown in the right. Four packets are indicated by red horizontal bars in the B1 panel. Panels (b–e) show the waveform (top) and frequency variations (bottom) for the four subelements. The blue dotted horizontal line in panel (b) through (e) is the mean value of frequencies for each subelement. The calculated mean values and standard deviations (σ) are given at the bottom of each panel.

Although the rise of these four subelements is a bit higher than the average frequency at the ends of the subelements analyzed, the rise is quite slight. The rise does not reach the average frequency of the next subelement to come. Thus there must be more frequency shifts occurring at either the ends of the subelements or in the gaps. See the “Supporting Information S1” section for more details of the long duration window data of Figure 4a. In general, the subelements analyzed are monochromatic ($\sigma \leq 1\%$), at least in the major portion of the subelements where the wave amplitudes are maximum.

Figures 5a–5c illustrate the dynamic spectrogram of a rising-tone chorus event that contains both lower and upper frequency bands. This event occurred on 13 April 2013 at $L = 5.5$ and a MLT of ~ 1.0 hr. The spacecraft MLAT was $\sim 5.7^\circ$. In the case, the lower band portion ranges from $\sim 1,200$ to $2,200$ Hz, and the upper band portion ranges from $\sim 2,500$ to $3,300$ Hz. The gap between the two bands from $\sim 2,200$ to $2,500$ Hz is at $f \sim 0.5f_{ce}$. The lower

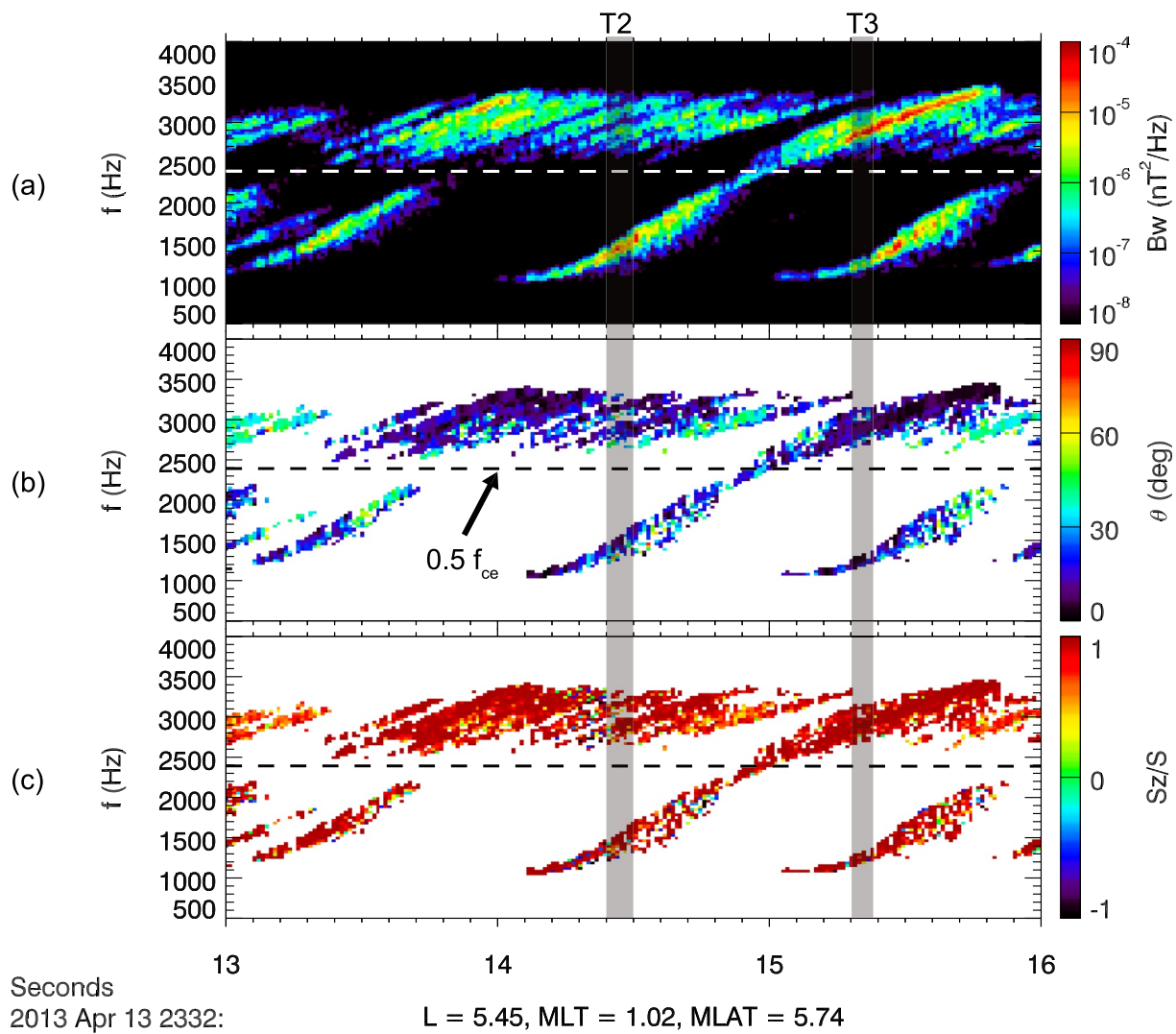


Figure 5. Rising-tone chorus elements detected at ~23:32 UT on 13 April 2013. The figure format is the same as in Figure 3. Two intervals T2 and T3 (vertical gray shadings) are selected for detailed analyses.

band portion of the element is apparently connected to an upper band portion of the element. Both the lower and upper bands of the chorus wave are propagating with wave normal angles less than 30° (Figure 5b). The waves are propagating away from the equatorial region, as expected (illustrated by the value of Sz/S in Figure 5c). Therefore, this is a “Type 1” chorus case.

Figure 6 shows a detailed view of the lower frequency band element marked by T2 in Figure 5. The waveform of the element is composed by several subelements. Each subelement or wave packet starts with a small amplitude, grows with time to a larger amplitude and then decreases with time to a smaller amplitude. The similarity in the amplitude profiles of the B1 and B2 components indicates that the waveforms are circularly polarized waves. Four subelements are indicated by red horizontal bars to be analyzed in further detail.

Figures 6b–6e illustrate the analysis results of the four subelements identified in Figure 5. The averaged wave normal (k) angle of four subelements are $\sim 33.9^\circ$, $\sim 12.3^\circ$, $\sim 7.8^\circ$, and $\sim 11.8^\circ$, respectively (not shown). For each subelement (each of the panels b through e), the frequency value is estimated based on the zero crossings of the B1 component. The mean value of frequencies for the four subelements are indicated by dashed horizontal lines. The average frequencies are: $\sim 1,382$, $\sim 1,437$, $\sim 1,482$, and $1,539$ Hz, respectively. The chorus subelements step up in frequency with time, as expected for a chorus riser tone. If the section of the lower band chorus portion of the element rises from $\sim 1,100$ to $\sim 2,200$ Hz in ~ 0.5 s, the “chirping rate” is $\sim 2,200$ Hz/s.

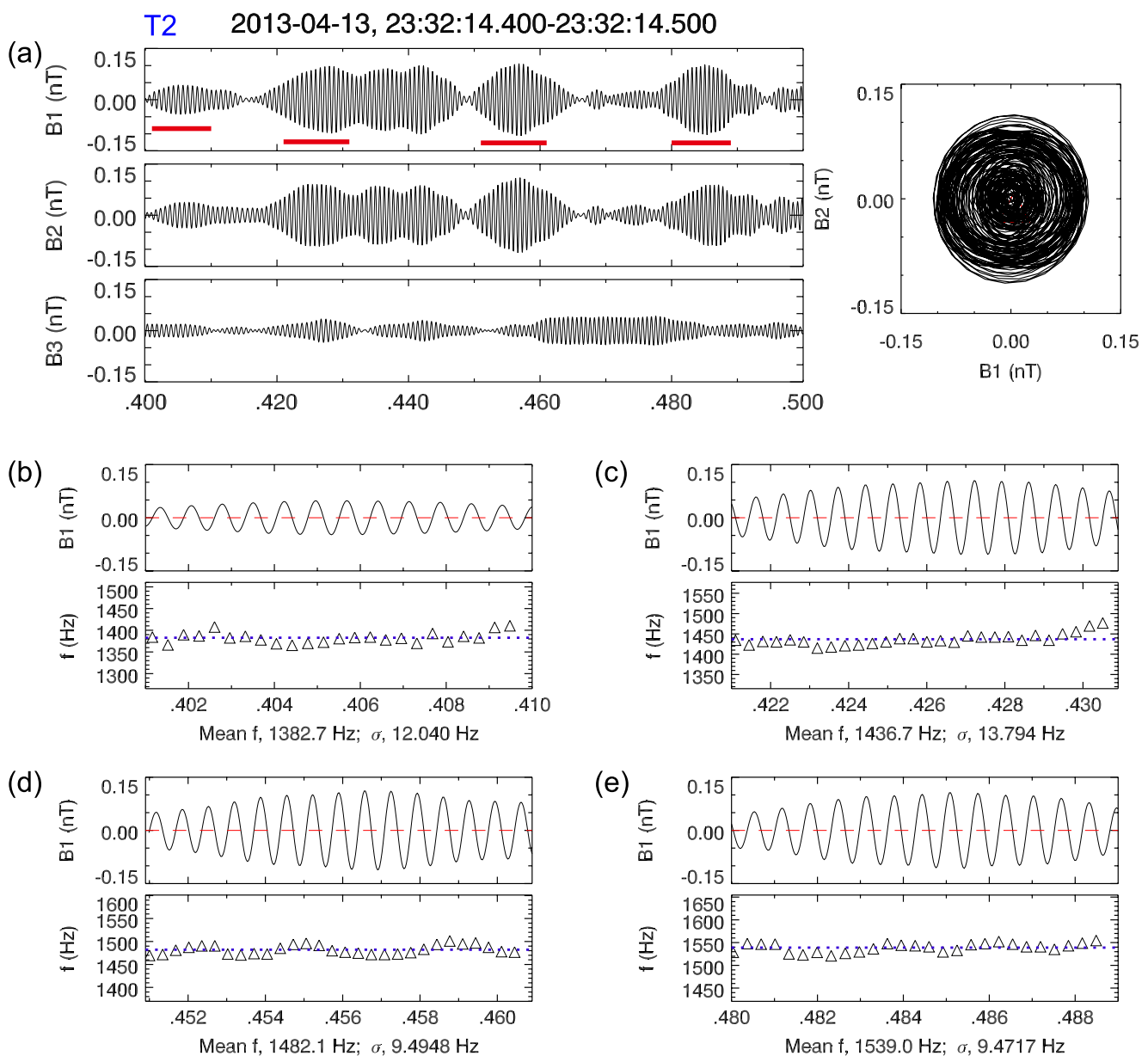


Figure 6. The T2 interval (Figure 5) waveforms of lower band chorus waves passed through a bandpass filter. Signals with frequencies between 800 and 2,400 Hz were passed. The format is the same as in Figure 4.

The frequency variances for the four subintervals are $\sim 0.9\%$, $\sim 1.0\%$, $\sim 0.6\%$ and $\sim 0.6\%$, respectively. The subelement in Figure 6b started at the average value, oscillated both above and below the average value and ended slightly above the average. The subelement shown in Figure 6c started at the average frequency, oscillated below the average, then near the average and ended up slightly above average. The subelement in Figure 6d started with a frequency below the average value, oscillated above and below the average several times and then ended at below average at essentially the same value as it initially started at. The subelement in Figure 6e started at the average frequency oscillated slightly above and below average several times and ended up at approximately the same frequency that it began at. The best description of the four subelements is that they were all monochromatic ($\sigma \leq 1\%$) in nature.

Similar to the subelements in Figure 4, the wave frequency varied smoothly from one half cycle to the next. There were no large statistical jumps from half cycle to half cycle. The wave frequencies in all four subelements (but particularly in Figures 6d and 6e) seem to again exhibit wave-like oscillations around the mean value.

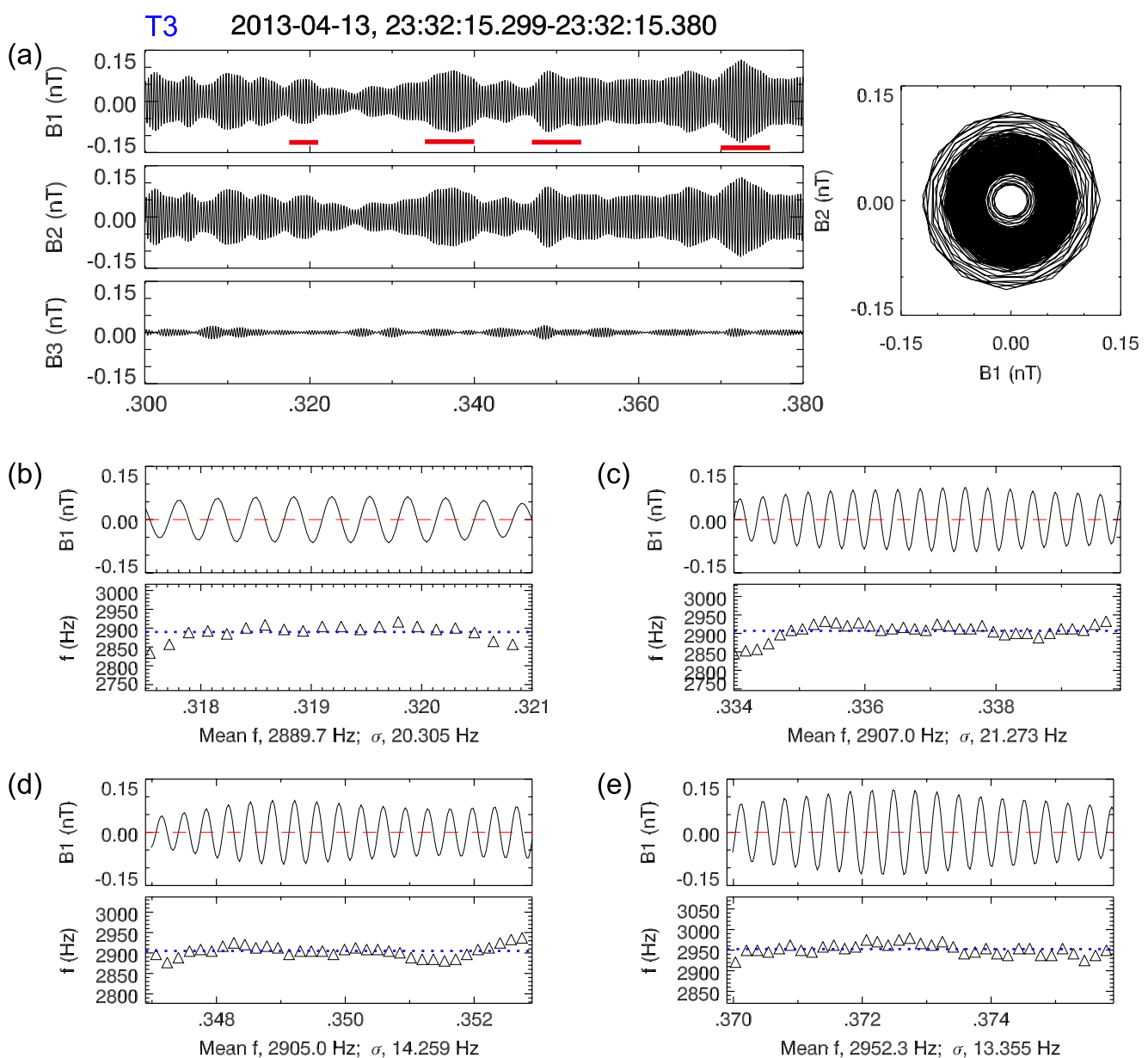


Figure 7. The format is the same as in Figure 4. The T3 interval (Figure 5) waveforms of upper band chorus waves were run through a filter allowing passage of frequencies between 2,400 and 3,600 Hz.

Figure 7 shows a similar wave analysis process for the T3 upper band element in Figure 5. This upper band element is also composed of many subelements, even though the boundaries between one subelement and the adjacent subelement are not clear. There are many more subelements for this upper band than for the lower band chorus shown in Figure 6. Four subelements are also selected to analyze the frequency variations (indicated by the red horizontal bars in Figure 7a). The averaged wave normal angles of the four subelements are $\sim 7.0^\circ$, $\sim 5.0^\circ$, $\sim 3.9^\circ$, and $\sim 6.9^\circ$, respectively. Their frequencies are $\sim 2,890$, $\sim 2,907$, $\sim 2,905$, and $2,952$ Hz, respectively. It is noticed that the second and third subelements have mean frequencies close to $\sim 2,900$ Hz. The third subelement was detected 0.013 s later in time than the second one. If the section of the upper band chorus portion of the element rises from $\sim 2,700$ to $\sim 3,500$ Hz in ~ 0.5 s, the “chirping rate” is $\sim 1,600$ Hz/s.

Figure 8 shows another rising-tone chorus event, which was observed at MLAT = 1.1° , MLT = 3.1 hr and $L = 5.5$. There are six nearly identical rising-tone elements. Here the first four rising-tone events have no power gaps at $f = 0.5f_{ce}$. The fifth and sixth elements have only upper bands. All six rising-tone elements are propagating with

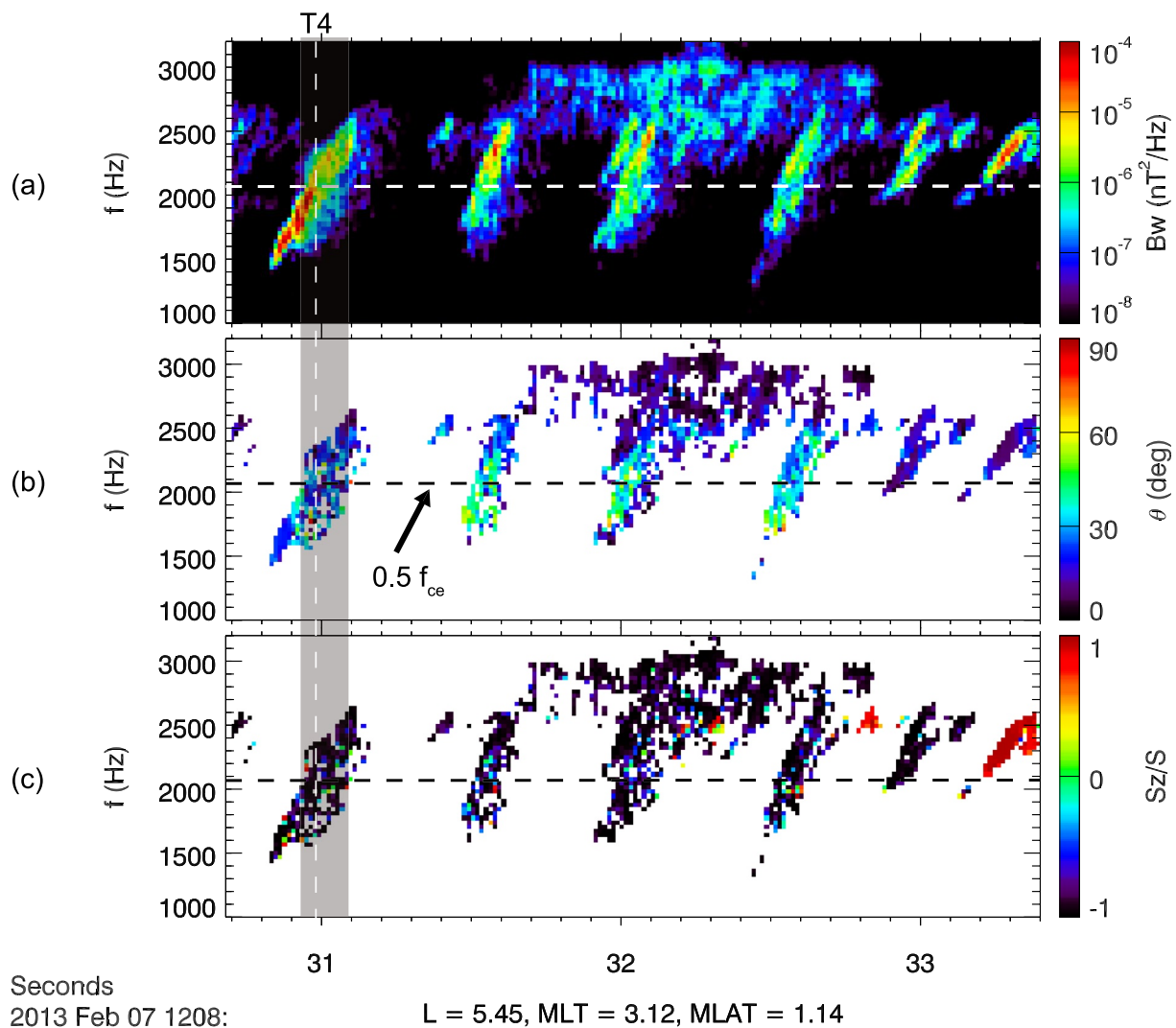


Figure 8. Rising-tone chorus elements for which there are no strong power gaps at $\sim 0.5f_{ce}$ (horizontal dashed lines in the three panels), or gap chorus. The figure format is the same as in Figure 3. One interval with no power gap (T4) was selected for detailed analyses.

wave normal angles $\leq 30^\circ$ (Figure 8b). In order to make comparisons with the two-band (Figure 5) and only upper band (Figure 3) types, one rising-tone element with no power gap (T4) was selected for detailed analyses. The frequency of the interval ranges from $\sim 1,800$ to $\sim 2,400$ Hz. The $0.5f_{ce}$ value corresponds to $\sim 2,100$ Hz and is indicated by a dashed horizontal line in all three panels.

Figure 9 shows the waveform of the entire rising-tone element (T4) identified in Figure 8. The element is composed of many small-interval subelements. The amplitudes of the subelements are largest at the lowest frequencies (the beginning of the interval from 12:08:30.93 to $\sim 12:08:30.96$ UT). After this interval, the peak amplitudes of the subelements are more or less constant until the end of the interval (12:08:31.089 UT). There is no obvious power gap in this latter interval. For reference, the $f = 0.5f_{ce}$ point would have occurred at $\sim 12:08:30.98$ UT. This is indicated by a vertical line in the figure. If the chorus element rises from $\sim 1,400$ to $\sim 2,600$ Hz in ~ 0.28 s, the chirping rate is $\sim 4,286$ Hz/s.

Figures 9b–9e show the frequency variations of four subelements in the T4 interval, respectively. The number of cycles analyzed are 13, 10, 9 and 10, respectively. The wave normal angles were 26.1° , 20.3° , 4.3° and 17.7° for the four subelements, respectively. In Figure 9b, the frequency starts slightly above the average for the interval and ends slightly below the average. The frequencies in Figure 9c are similar in nature to Figure 9b with a slightly different ending. The wave frequency starts slightly above the average value then smoothly oscillates around

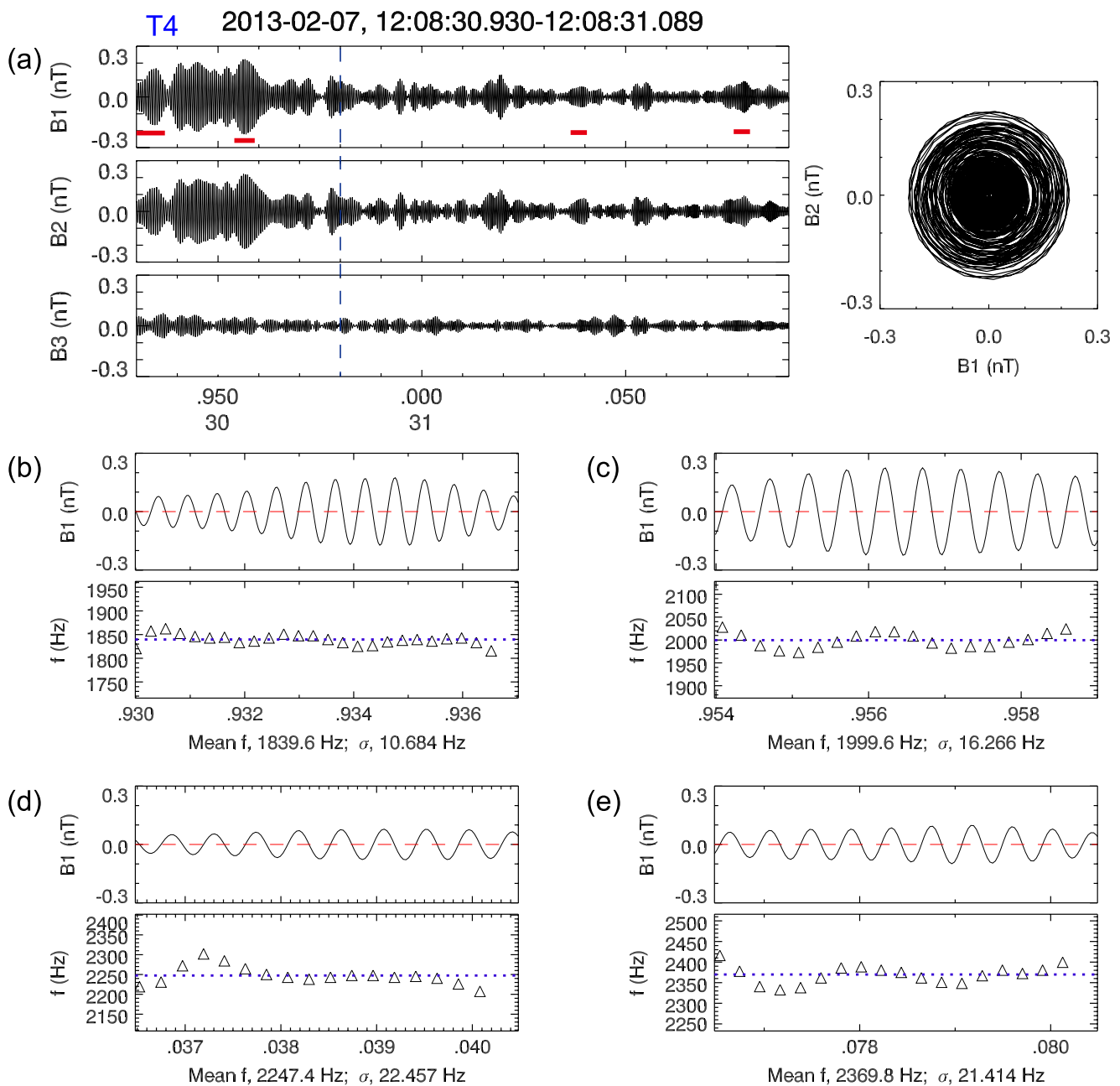


Figure 9. The waveforms of the T4 interval shown in Figure 8. The format is the same as in Figure 4. Waves with frequencies between $\sim 1,200$ and $\sim 2,900$ Hz were passed through the filter, that is, the microstructure of the entire rising element is shown. A vertical blue line indicates the chorus frequency where $f \sim 0.5f_{ce}$.

the average value and then ends at approximately the same value as it started. Figure 9d is different from either Figure 9b or Figure 9c. The frequency starts below the average value, oscillates around the mean and then ends up below the average. Figure 9e is similar to Figure 9c. The frequency starts above the average value, oscillates both above and below the mean and then ends with frequencies above the mean. The variances of the frequencies for the four subelements are 0.6%, 0.8%, 1.0%, and 0.9%, respectively. The subelements are monochromatic with nearly constant frequencies. These results for the “no gap” rising tone of Figure 8 are similar to that of the upper band event in Figure 3 and “Type 1” two-frequency chorus event in Figure 5.

Figure 10 presents two-frequency chorus waves, where the lower band waves ($\sim 1,300$ – $1,900$ Hz) exhibit discrete rising tones and the upper band waves ($\sim 2,100$ – $2,400$ Hz) is more of a hiss-like structure with some dot-like

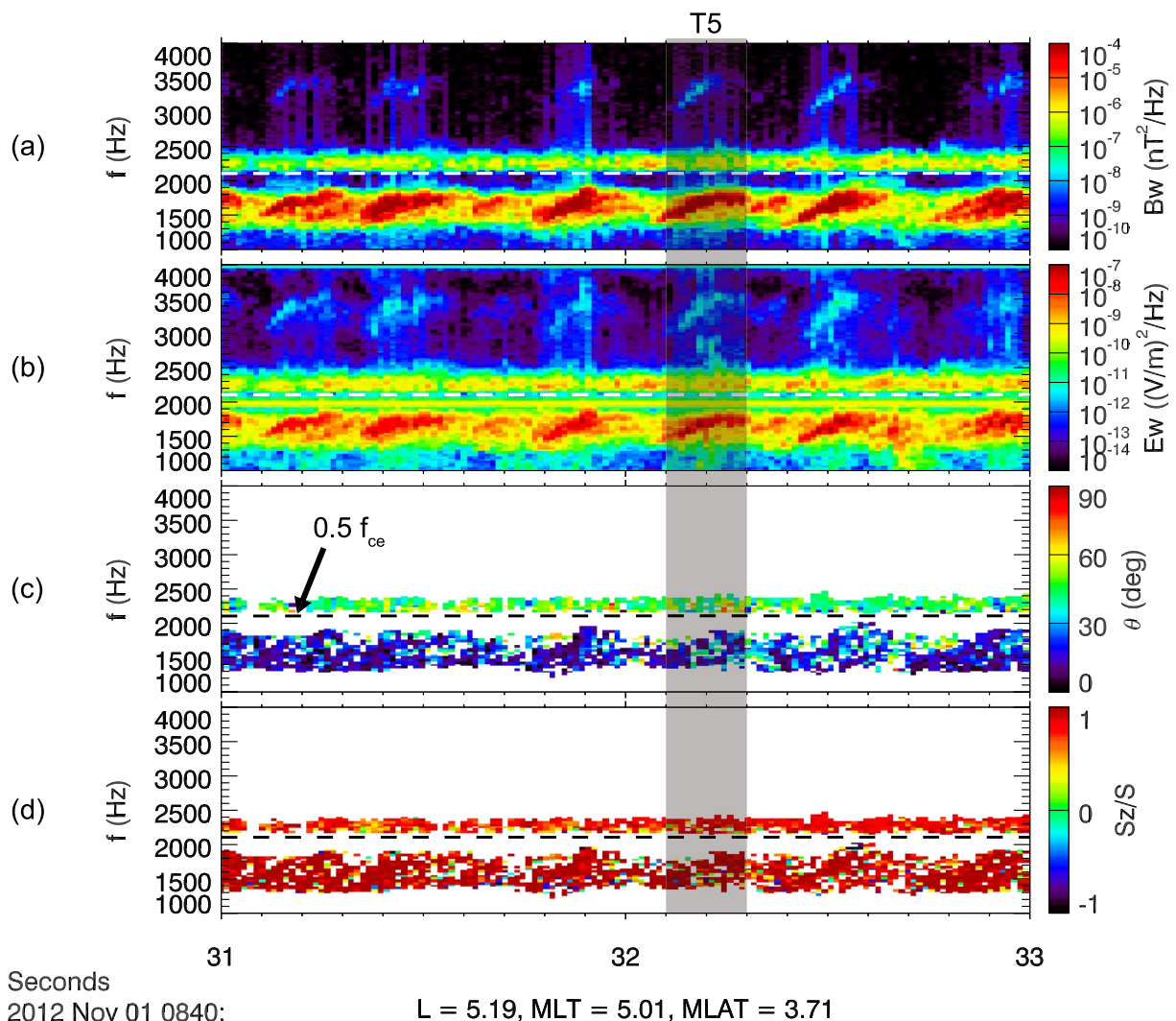


Figure 10. Two-frequency chorus waves, where the lower band waves exhibit discrete rising tones and the upper band waves have hiss-like structure with some intense “dots.” (a) Wave magnetic power spectrum, (b) wave electrostatic power spectrum, (c) wave normal angle relative to the background magnetic field B_0 , and (c) the ratio S_z/S . The horizontal dashed lines in each of the four panels represent $0.5f_{ce}$ and $1.0f_{ce}$, respectively.

intensifications (Figures 10a and 10b). This case is somewhat similar to the two-frequency chorus in Figure 1. However here there is no clear connection between the lower band risers and the intense upper band “dots.” The lower-band chorus waves are found to have small wave normal angles, that is, less than $\sim 30^\circ$, while the upper-band chorus waves have relatively larger wave normal angles, that is, $\sim 40^\circ$. In order to compare the two bands of chorus waves, the interval T5 was selected to perform further analyses. The chirping rate is $\sim 3,000$ Hz/s for the lower band elements.

The waveform analyses of interval T5 for lower band and upper band chorus waves are presented in Figures 11 and 12, respectively. The waveforms of the lower band and upper band chorus waves are composed of many small subelements (Figures 11a and 12a). The frequency variations of four subelements in the T5 interval for lower band and upper band waves are shown in Figures 11b–11e and Figures 12b–12e, respectively. The frequency variations are quite different from event to event.

In Figure 11, the wave normal angles of the four selected subelements were 9.6° , 10.7° , 27.3° and 21.1° , respectively. In Figure 12, the wave normal angles of the four subelements were 51.3° , 40.5° , 45.9° and 38.6° , respectively. In Figure 11b, the frequency starts slightly below the average value and ends slightly above the average. It has a more or less monotonic increase. For Figure 11c, the frequency starts at the average value, then goes slightly

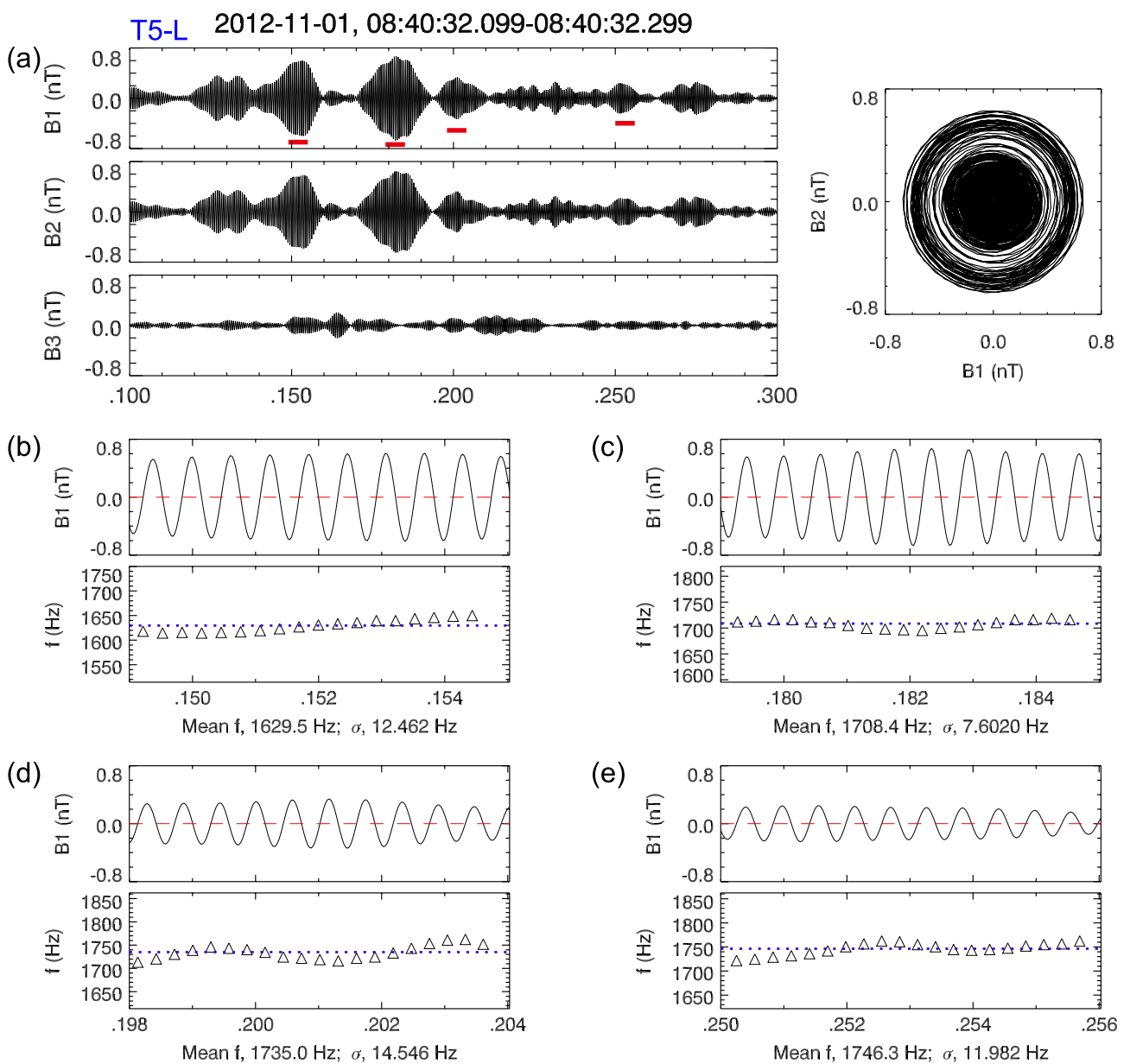


Figure 11. The format is the same as in Figure 4. The T5 interval (Figure 10) waveforms of lower band chorus waves passed through a bandpass filter (1,200–2,000 Hz).

below average and ends at the average value. For Figure 11d, the frequency starts below the average, oscillates above average twice and then ends up at the average value. The frequency in Figure 11e starts below the average value, oscillates to slightly above, then below the average value and ends up slightly above the average. The variances for the four subelements were 0.8%, 0.5%, 0.8% and 0.7%, respectively.

In Figure 12b, the frequency starts slightly below average, oscillates above and below once and ends up at the average value. In Figure 12c, the frequency starts at slightly above average and maintains that value through more than half of the interval and then decreases monotonically to end up below average. Figure 12d starts with the frequency slightly below average and then is above average for half of the interval, and then ends up below average. Figure 12e shows that the frequency starts slightly above the average, then decreases below the average and then stays at a more or less constant value. It ends up slightly below the average value. The variances for the four subelement intervals are 0.3%, 0.6%, 0.4% and 0.4%, respectively.

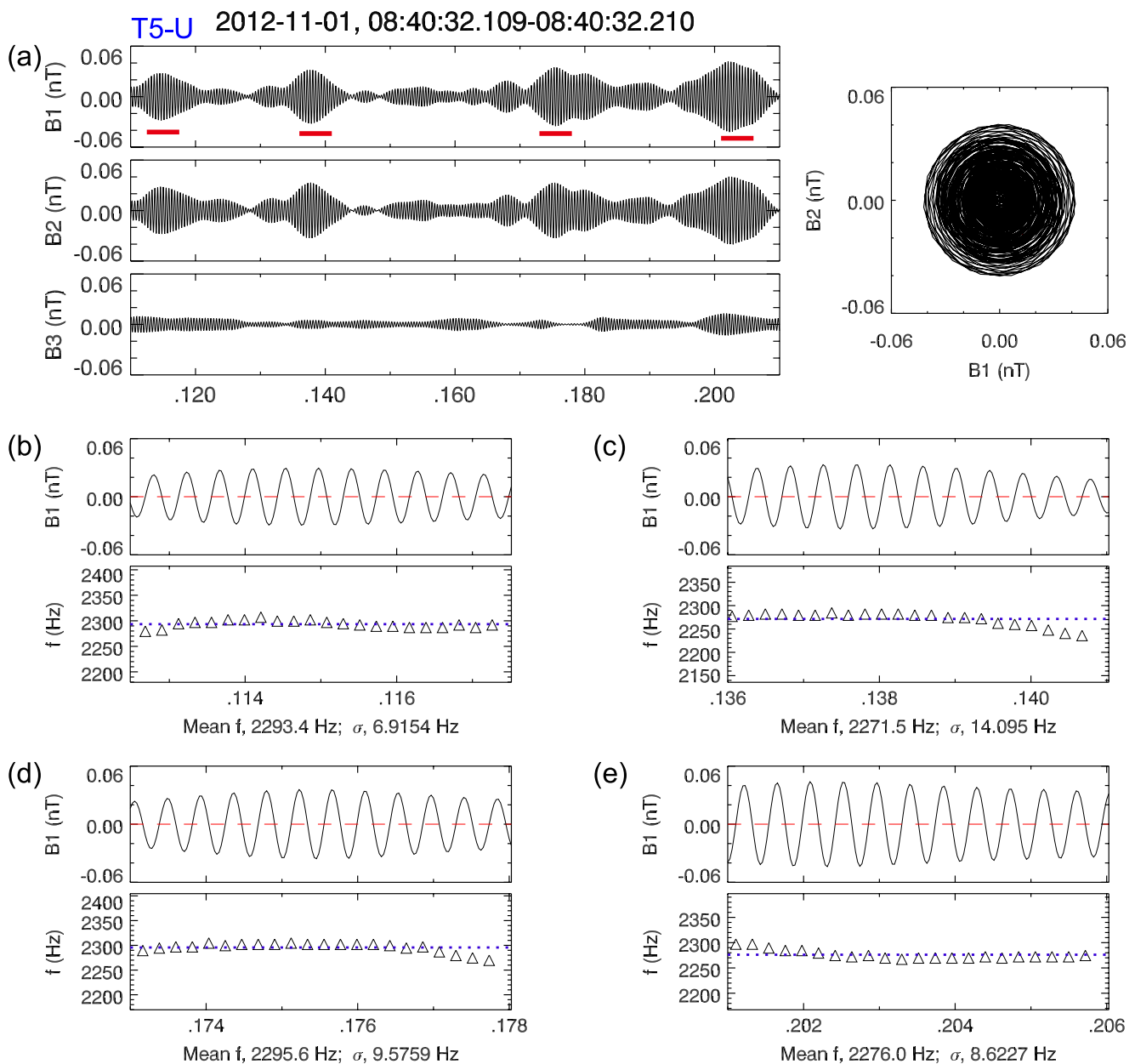


Figure 12. The format is the same as in Figure 4. The T5 interval (Figure 10) waveforms of upper band chorus waves were passed through a bandpass filter, that is, between 2,000 and 2,600 Hz.

The subelements are also monochromatic with nearly constant frequencies. These results for the “Type 2” two-frequency chorus waves of Figure 10 are similar to other events analyzed in the paper. The eight subelements shown in Figures 11 and 12 displayed wave-like frequency signatures which were apparently not statistical type fluctuations. This is similar to the eight subelements shown previously. The waveform analysis for the second harmonic can be found in the “Supporting Information S1.”

The summary information of four types of rising-tone chorus waves and their subelements are presented in Table 1. All of the chorus waves analyzed in this study were located at the near-equatorial region (with $|MLAT| < 6.0^\circ$), and in the midnight to dawn sector. Four chorus waves present as different types, including only upper band, Type 1, no gap, and Type 2. We have analyzed 24 subelements from the upper band, lower band and near $0.5 f_{ce}$ (gap) chorus of four wave elements. All of the subelements are nearly monochromatic with $\sigma \leq 1\%$.

Table 1

Summary of Four Rising-Tone Chorus Waves and Their Subelements

Chorus waves					Subelements	Average frequency (σ) (Hz)			
No.	Type	MLT	L	MLAT ($^{\circ}$)	No./type	S1	S2	S3	S4
1	Only upper band	1.5	5.3	-1.8	T1/upper	2,726 (12.6)	2,786 (7.9)	2,836 (14.3)	2,929 (9.4)
2	Type 1	1.0	5.5	5.7	T2/lower	1,383 (12.0)	1,437 (13.8)	1,482 (9.5)	1,539 (9.5)
					T3/upper	2,890 (20.3)	2,907 (21.3)	2,905 (14.3)	2,952 (13.4)
3	No gap	3.1	5.5	1.1	T4/ $\sim 0.5f_{ce}$	1,840 (10.7)	2,000 (16.3)	2,247 (22.4)	2,370 (21.4)
4	Type 2	5.0	5.2	3.7	T5/lower	1,630 (12.5)	1,708 (7.6)	1,735 (14.5)	1,746 (12.0)
					T6/upper	2,293 (6.9)	2,272 (14.1)	2,296 (9.6)	2,276 (8.6)

4. Summary and Conclusions

To make comparisons of Type 1 upper band chorus structure and substructure to lower band chorus, rising tone elements which had power gap at $\sim 0.5f_{ce}$ (Figure 5) were analyzed in detail. From our analyses, it was found that the nature of Type 1 upper band chorus is the same as lower band chorus: Type 1 upper band chorus is composed of short duration subelements (the same structure) and the substructures are monochromatic (the same substructures) in nature.

A chorus riser element that had continuous wave power from $f < 0.5f_{ce}$ to $f > 0.5f_{ce}$ was analyzed (Figure 8). It was found that the nature of gap ($f \sim 0.5f_{ce}$) chorus waves were the same as lower band and upper band chorus. The $\sim 0.5f_{ce}$ chorus was composed of short-duration subelements (the same substructure) and the subelements were monochromatic.

We selected 20 intense rising tone chorus intervals (not all shown) that were located in the midnight-to-dawn local time sector and near the magnetic equator, $|MLAT| < 10^{\circ}$. For the 20 intervals, the elements were found to be composed of short-duration monochromatic subelements/packets.

What can one conclude from the above results? One obvious strong possibility is that the mechanism of wave generation for Type 1 upper band chorus, lower band chorus and $\sim 0.5f_{ce}$ gap chorus are probably all the same. From the Kennel-Petschek instability theory, the only difference will be the resonant energetic electrons involved in the particular wave frequency generated. The Type 1 upper band chorus would be generated by the lowest energy part of the $\sim 10\text{--}100$ keV substorm-injected temperature anisotropic electrons.

The identification of monochromatic subelements within the $f \sim 0.5f_{ce}$ gap is consistent with the above scenario. The anisotropic substorm-injected energetic electrons generate the short duration monochromatic subelements for all frequencies of the riser. Then Landau/cyclotron damping typically eliminates some of the waves, creating the power gap.

A Type 2 upper band chorus event (Fu et al., 2014) was studied. The upper band did not show any obvious relationship to the lower band, the definition of Type 2 chorus. The upper band was found to be composed of monochromatic subelements. Thus if it is correct that the upper band chorus is sometimes generated by a different population of energetic electrons with different temperature (and pitch angle?) distributions (Fu et al., 2014; Liu et al., 2011), then that mechanism must involve electron phase bunching, just as the case for Type 1 chorus. We should mention that the Type 2 case in Figure 10 is not the same as the typical Type 2 case shown in Figure 2. We were not able to find a case similar to Figure 2 in the Van Allen Probes data (searching from more than 2 years of data).

4.1. Final Comments

Previous models and simulations can reproduce the subelements within chorus elements Hanzelka et al., (2020, 2021; Ke et al., 2017; Tao et al., 2017), but the fundamental physics behind the formation of subelements is still unclear. Santolík (2008) mentioned that the beating effect of simultaneously present signatures at closely separated frequencies could explain the nature of the subelements. Zhang et al. (2020) statistically analyzed the frequency variation and lengths of the subelements, and supported the premise that the structure can be

formed by the superposition of different frequency waves. By conducting test particle simulations, Hanzelka et al. (2021) have shown that the electron distribution carries an imprint of the subelements within rising-tone chorus elements. Tsurutani et al. (2020) have mentioned that nearly monochromatic subelements are most likely excited by a narrow energy range of phase bunched energetic electrons. The higher frequency subelements in a rising-tone element should be excited by a lower-energy range of energetic electrons, while the lower frequency subelements should be excited by a higher-energy range of electrons. Until now, there is no widely accepted explanation for how and why the subelements form within chorus element. An examination of energetic electrons during chorus events will be helpful in making progress with this problem.

Additionally more advanced computer modeling needs to be performed with corresponding observational evidence to support the findings. Wave-like structures were noted in the wave frequencies of the subelements. This seemed to be present in 16 subelements studied. This feature is not understood at this time. Perhaps modeling can explain these features.

A theory explaining chorus rising tones should also be able to explain why the same or very similar frequency-time profiles of the risers occur for hours within the same drifting electron cloud. Free energy must be being supplied to the electrons within the cloud as the electrons drift from the midnight sector toward dawn (Tsurutani et al., 2020). We hope that fellow scientists will be able to advance the Kennel and Petschek (1966) theory to explain all the various facets of the chorus rising tone subelements.

Data Availability Statement

The RBSP data used in this study are available from the website: <https://spdf.gsfc.nasa.gov/pub/data/rbsp/>. SPEDAS is available at <http://themis.ssl.berkeley.edu/socware/>.

Acknowledgments

This research was funded by the Strategic Priority Research Program of Chinese Academy of Sciences Grant Nos. XDB41000000, the NSFC Grant 41774151, 41631071, Key Research Program of Frontier Sciences CAS (QYZDJ-SSW-DQC010), the Fundamental Research Funds for the Central Universities (WK3420000013), and “USTC Tang Scholar” program. Work performed by RH was funded by the Science and Engineering Research Board (SERB Grant No. SB/S2/RJN-080/2018), a statutory body of the Department of Science and Technology (DST), Government of India through the Ramanujan Fellowship. GSL thanks the Indian National Science Academy, New Delhi for the support under the INSA-Honorary Scientist Scheme. We also acknowledge the entire RBSP instrument teams.

References

- Bell, T. F., Inan, U. S., Haque, N., & Pickett, J. S. (2009). Source regions of banded chorus. *Geophysical Research Letters*, 36(11), L11101. <https://doi.org/10.1029/2009GL037629>
- Bellan, P. M. (2013). Pitch angle scattering of an energetic magnetized particle by a circularly polarized electromagnetic wave. *Physics of Plasmas*, 20(4), 042117. <https://doi.org/10.1063/1.4801055>
- Burtis, W. J., & Helliwell, R. A. (1969). Banded chorus a new type of VLF radiation observed in the magnetosphere by OGO 1 and OGO 3. *Journal of Geophysical Research*, 74(11), 3002–3010. <https://doi.org/10.1029/JA074i011p03002>
- Chen, H., Gao, X., Lu, Q., Fan, K., Ke, Y., Wang, X., & Wang, S. (2022a). Gap formation around $0.5\Omega_e$ in the whistler-mode waves due to the plateau-like shape in the parallel electron distribution: 2D PIC simulations. *Journal of Geophysical Research: Space Physics*, 127(5), e2021JA030119. <https://doi.org/10.1029/2021JA030119>
- Chen, H., Gao, X., Lu, Q., Sauer, K., Chen, R., Yao, J., & Wang, S. (2021). Gap formation around $0.5\Omega_e$ of whistler-mode waves excited by electron temperature anisotropy. *Journal of Geophysical Research: Space Physics*, 126(2), e2020JA028631. <https://doi.org/10.1029/2020JA028631>
- Chen, H., Lu, Q., Wang, X., Fan, K., Chen, R., & Gao, X. (2022). One-dimensional gcPIC-8f simulation of hooked chorus waves in the Earth’s inner magnetosphere. *Geophysical Research Letters*, 49(4), e2022GL097989. <https://doi.org/10.1029/2022GL097989>
- Coroniti, F. V., Scarf, F. L., Kennel, C. F., & Kurth, W. S. (1984). Analysis of chorus emissions at Jupiter. *Journal of Geophysical Research*, 89(A6), 3801. <https://doi.org/10.1029/JA089iA06p03801>
- Frandsen, A. M. A., Holzer, R. E., & Smith, E. J. (1969). Ogo search coil magnetometer experiments. *IEEE Transactions on Geoscience Electronics*, 7(2), 61–74. <https://doi.org/10.1109/TGE.1969.271324>
- Fu, X., Cowee, M. M., Friedel, R. H., Funsten, H. O., Gary, S. P., Hospodarsky, G. B., et al. (2014). Whistler anisotropy instabilities as the source of banded chorus: Van Allen Probes observations and particle-in-cell simulations. *Journal of Geophysical Research: Space Physics*, 119(10), 8288–8298. <https://doi.org/10.1002/2014JA020364>
- Gao, X. L., Chen, L. J., Li, W., Lu, Q. M., & Wang, S. (2019). Statistical results of the power gap between lower-band and upper-band chorus waves. *Geophysical Research Letters*, 46(8), 4098–4105. <https://doi.org/10.1029/2019GL082140>
- Gao, X. L., Chen, R., Lu, Q. M., Chen, L. J., Chen, H. Y., & Wang, X. Y. (2022). Observational evidence for the origin of repetitive chorus emissions. *Geophysical Research Letters*, 49(12), e2022GL099000. <https://doi.org/10.1029/2022GL099000>
- Gao, X. L., Lu, Q. M., Bortnik, J., Li, W., Chen, L. J., & Wang, S. (2016). Generation of multiband chorus by lower band cascade in the Earth’s magnetosphere. *Geophysical Research Letters*, 43(6), 2343–2350. <https://doi.org/10.1002/2016GL068313>
- Hanzelka, M., Santolík, O., Omura, Y., & Kolmašová, I. (2021). Measurability of the nonlinear response of electron distribution function to chorus emissions in the Earth’s radiation belt. *Journal of Geophysical Research: Space Physics*, 126(9), e2021JA029624. <https://doi.org/10.1029/2021JA029624>
- Hanzelka, M., Santolík, O., Omura, Y., Kolmašová, I., & Kletzing, C. A. (2020). A model of the subpacket structure of rising tone chorus emissions. *Journal of Geophysical Research: Space Physics*, 125(8), e2020JA028094. <https://doi.org/10.1029/2020JA028094>
- Hosokawa, K., Miyoshi, Y., Ozaki, M., Oyama, S.-I., Ogawa, Y., Kurita, S., et al. (2020). Multiple time-scale beats in aurora: Precise orchestration via magnetospheric chorus waves. *Scientific Reports*, 10(1), 3380. <https://doi.org/10.1038/s41598-020-59642-8>
- Ke, Y., Gao, X., Lu, Q., Wang, X., & Wang, S. (2017). Generation of rising-tone chorus in a two-dimensional mirror field by using the general curvilinear PIC code. *Journal of Geophysical Research: Space Physics*, 122(8), 8154–8165. <https://doi.org/10.1002/2017JA024178>
- Kennel, C. F., & Petschek, H. E. (1966). Limit on stably trapped particle fluxes. *Journal of Geophysical Research*, 71(1), 1–28. <https://doi.org/10.1029/JZ071i001p00001>

- Kletzing, C. A., Kurth, W. S., Acuna, M., MacDowall, R. J., Torbert, R. B., Averkamp, T., et al. (2013). The electric and magnetic field instrument suite and integrated science (EMFISIS) on RBSP. *Space Science Reviews*, 179(1–4), 127–181. <https://doi.org/10.1007/s11214-013-9993-6>
- Kurita, S., Katoh, Y., Omura, Y., Angelopoulos, V., Cully, C. M., Le Contel, O., & Misawa, H. (2012). THEMIS observation of chorus elements without a gap at half the gyrofrequency. *Journal of Geophysical Research*, 117(A11), A11223. <https://doi.org/10.1029/2012JA018076>
- Lakhina, G. S., Tsurutani, B. T., Verkhoglyadova, O. P., & Pickett, J. S. (2010). Pitch angle transport of electrons due to cyclotron interactions with the coherent chorus subelements. *Journal of Geophysical Research*, 115(A8), A00F15. <https://doi.org/10.1029/2009JA014885>
- Lauben, D. S., Inan, U. S., Bell, T. F., & Gurnett, D. A. (2002). Source characteristics of ELF/VLF chorus. *Journal of Geophysical Research*, 107(A12), 1429. <https://doi.org/10.1029/2000JA003019>
- LeDocq, M. J., Gurnett, D. A., & Hospodarsky, G. B. (1998). Chorus source locations from VLF Poynting flux measurements with the Polar spacecraft. *Geophysical Research Letters*, 25(21), 4063–4066. <https://doi.org/10.1029/1998GL900071>
- Li, J., Bortnik, J., An, X., Li, W., Angelopoulos, V., Thorne, R. M., et al. (2019). Origin of two-band chorus in the radiation belt of Earth. *Nature Communications*, 10(1), 4672. <https://doi.org/10.1038/s41467-019-12561-3>
- Li, W., Bortnik, J., Thorne, R. M., & Angelopoulos, V. (2011). Global distribution of wave amplitudes and wave normal angles of chorus waves using THEMIS wave observations. *Journal of Geophysical Research*, 116(A12), A12205. <https://doi.org/10.1029/2011JA017035>
- Liu, K., Gary, S. P., & Winske, D. (2011). Excitation of banded whistler waves in the magnetosphere. *Geophysical Research Letters*, 38(14), L14108. <https://doi.org/10.1029/2011GL048375>
- Lu, Q., Chen, L., Wang, X., Gao, X., Lin, Y., & Wang, S. (2021). Repetitive emissions of rising-tone chorus waves in the inner magnetosphere. *Geophysical Research Letters*, 48(15), e2021GL094979. <https://doi.org/10.1029/2021GL094979>
- Maeda, K. (1976). Cyclotron side-band emissions from ring-current electrons. *Planetary and Space Science*, 24(4), 341–347. [https://doi.org/10.1016/0032-0632\(76\)90045-3](https://doi.org/10.1016/0032-0632(76)90045-3)
- Meredith, N. P., Horne, R. B., & Anderson, R. R. (2001). Substorm dependence of chorus amplitudes: Implications for the acceleration of electrons to relativistic energies. *Journal of Geophysical Research*, 106(A7), 13165–13178. <https://doi.org/10.1029/2000JA000156>
- Omura, Y. (2021). Nonlinear wave growth theory of whistler-mode chorus and hiss emissions in the magnetosphere. *Earth Planets and Space*, 73(1), 95. <https://doi.org/10.1186/s40623-021-01380-w>
- Omura, Y., Hikishima, M., Katoh, Y., Summers, D., & Yagitani, S. (2009). Nonlinear mechanisms of lower-band and upper-band VLF chorus emissions in the magnetosphere. *Journal of Geophysical Research*, 114(A7), A07217. <https://doi.org/10.1029/2009JA014206>
- Ratcliffe, H., & Watt, C. E. J. (2017). Self-consistent formation of a 0.5 cyclotron frequency gap in magnetospheric whistler mode waves. *Journal of Geophysical Research: Space Physics*, 122(8), 8166–8180. <https://doi.org/10.1002/2017JA024399>
- Russell, C. T., Holzer, R. E., & Smith, E. J. (1969). Ogo 3 observations of elf noise in the magnetosphere: 1. Spatial extent and frequency of occurrence. *Journal of Geophysical Research*, 74(3), 755–777. <https://doi.org/10.1029/JA074i003p00755>
- Santolík, O. (2008). New results of investigations of whistler-mode chorus emissions. *Nonlinear Processes in Geophysics*, 15(4), 621–630. <https://doi.org/10.5194/npg-15-621-2008>
- Santolík, O., Gurnett, D. A., Pickett, J. S., Parrot, M., & Cornilleau-Wehrlin, N. (2003). Spatio-temporal structure of storm-time chorus. *Journal of Geophysical Research*, 108(A7), 1278. <https://doi.org/10.1029/2002JA009791>
- Santolík, O., Kletzing, C. A., Kurth, W. S., Hospodarsky, G. B., & Bounds, S. R. (2014). Fine structure of large-amplitude chorus wave packets. *Geophysical Research Letters*, 41(2), 293–299. <https://doi.org/10.1002/2013GL058889>
- Schrivner, D., Ashour-Abdalla, M., Coroniti, F. V., LeBoeuf, J. N., Decyk, V., Travnick, P., et al. (2010). Generation of whistler mode emissions in the inner magnetosphere: An event study. *Journal of Geophysical Research*, 115(A8), A00F17. <https://doi.org/10.1029/2009JA014912>
- Smith, E. J., & Tsurutani, B. T. (1976). Magnetosheath lion roars. *Journal of Geophysical Research*, 81(13), 2261–2266. <https://doi.org/10.1029/JA081i013p02261>
- Sonnerup, B. U., & Cahill, L. J., Jr. (1967). Magnetopause structure and attitude from Explorer 12 observations. *Journal of Geophysical Research*, 72(1), 171–183. <https://doi.org/10.1029/JZ072i001p00171>
- Tao, X., Zonca, F., & Chen, L. (2017). Identify the nonlinear wave-particle interaction regime in rising tone chorus generation. *Geophysical Research Letters*, 44(8), 3441–3446. <https://doi.org/10.1002/2017GL072624>
- Teng, S., Tao, X., & Li, W. (2019). Typical characteristics of whistler mode waves categorized by their spectral properties using Van Allen Probes observations. *Geophysical Research Letters*, 46(7), 3607–3614. <https://doi.org/10.1029/2019GL082161>
- Thorne, R. M., Ni, B., Tao, X., Horne, R. B., & Meredith, N. P. (2010). Scattering by chorus waves as the dominant cause of diffuse auroral precipitation. *Nature*, 467(7318), 944–946. <https://doi.org/10.1038/nature09467>
- Tsurutani, B. T., Chen, R., Gao, X., Lu, Q., Pickett, J. S., Lakhina, G. S., et al. (2020). Lower-band “monochromatic” chorus riser subelement/wave packet observations. *Journal of Geophysical Research: Space Physics*, 125(10), e2020JA028090. <https://doi.org/10.1029/2020JA028090>
- Tsurutani, B. T., Lakhina, G. S., & Verkhoglyadova, O. P. (2013). Energetic electron (>10 keV) microburst precipitation, ~5–15 s X-ray pulsations, chorus and wave-particle interactions: A review. *Journal of Geophysical Research: Space Physics*, 118(5), 2296–2312. <https://doi.org/10.1002/jgra.50264>
- Tsurutani, B. T., & Smith, E. J. (1974). Postmidnight chorus: A substorm phenomenon. *Journal of Geophysical Research*, 79(1), 118–127. <https://doi.org/10.1029/JA079i001p00118>
- Tsurutani, B. T., & Smith, E. J. (1977). Two types of magnetospheric ELF chorus and their substorm dependences. *Journal of Geophysical Research*, 82(32), 5112–5128. <https://doi.org/10.1029/JA082i032p05112>
- Tsurutani, B. T., Smith, E. J., West, H. I., Jr., & Buck, R. M. (1979). Chorus, energetic electrons and magnetospheric substorms. In P. J. Palmadesso & K. Papadopoulos (Eds.), *Wave instabilities in space plasmas* (p. 55). D. Reidel.
- Tsurutani, B. T., Verkhoglyadova, O. P., Lakhina, G. S., & Yagitani, S. (2009). Properties of dayside outer zone chorus during HILDCAA events: Loss of energetic electrons. *Journal of Geophysical Research*, 114(A3), A03207. <https://doi.org/10.1029/2008JA013353>
- Verkhoglyadova, O. P., Tsurutani, B. T., & Lakhina, G. S. (2010). Properties of obliquely propagating chorus. *Journal of Geophysical Research*, 115(A9), A00F19. <https://doi.org/10.1029/2009JA014809>
- Zhang, X. J., Mourenas, D., Artemyev, A. V., Angelopoulos, V., Kurth, W. S., Kletzing, C. A., & Hospodarsky, G. B. (2020). Rapid frequency variations within intense chorus wave packets. *Geophysical Research Letters*, 47(15), e88853. <https://doi.org/10.1029/2020GL088853>